Applied Catalysis B: Environmental 223 (2018) 36–46

Contents lists available at ScienceDirect

Applied Catalysis B: Environmental

journal homepage: www.elsevier.com/locate/apcatb

Promotion effect of zirconia on Mg(Ni,Al)O mixed oxides derived from hydrotalcites in CO_2 methane reforming

Radosław Dębek[a,b,*], Monika Motak[a], Maria Elena Galvez[b], Teresa Grzybek[a], Patrick Da Costa[b]

[a] AGH University of Science and Technology, Faculty of Energy and Fuels, Department of Fuels Technology, al.A. Mickiewicza 30, 30-059, Kraków, Poland
[b] Sorbonne Universites, UPMC, Univ. Paris 6, CNRS, UMR 7190, Institut Jean Le Rond d'Alembert, 2 Place de la Gare de Ceinture, 78210 Saint-Cyr-L'Ecole, France

ARTICLE INFO

Article history:
Received 28 November 2016
Received in revised form 3 March 2017
Accepted 8 June 2017
Available online 9 June 2017

Keywords:
Carbon dioxide
Dry reforming of methane
Hydrotalcites
Nickel
Zirconia

ABSTRACT

Hydrotalcite-derived catalysts promoted with Zr species were prepared via co-precipitation method, resulting in materials with various Zr loading. Physicochemical properties of catalysts precursors and final catalysts were investigated via XRF, XRD, low temperature N_2 sorption, H_2-TPR, CO_2-TPD, TG, SEM and TEM techniques. So characterized catalysts were subsequently tested in the dry methane reforming reaction at 550 °C. Zr-loading introduced into brucite-like layers influenced the process of thermal decomposition of HTs and, as a result, their properties and performance in DRM. Although Zr promotion decreased activity, it strongly increased the stability and selectivity of the catalysts. The catalyst with Zr species present in the framework of periclase-like mixed oxide exhibited high resistance to coking due to the rearrangement of Ni particles upon DRM reaction.

1. Introduction

The so far proved increasing atmospheric CO_2 concentration has forced implementation of several strategies in the aim of controlling anthropogenic CO_2 emissions. These strategies include CCS (Carbon Capture and Sequestration) and CCU (Carbon Capture and Utilization) technologies [1,2]. The latter treats CO_2 as a valuable chemical feedstock and can be realized through different pathways. Moreover, the implementation of chemical CO_2 utilization technologies is seen nowadays as a key element towards our sustainable development and as a major step in our transition to a future renewable-based energy generation scenario. Therefore the research in this area of science and technology is essential and stays in line within the European Union policy and international agreements (i.e. COP21) [3,4]. Among the different routes for CO_2 chemical valorisation, dry reforming of methane (DRM) offers a number of remarkable advantages, i.e. the possibility of thermal energy storage (via CETS – Chemical Energy Transmission and Storage systems) directly linked to the production of a syngas containing an equimolar mixture of H_2 and CO [5–8]. However, DRM has not been yet commercialized, and this is due to the lack of stable catalysts, since the materials tested so far undergo fast deactivation mainly due to the formation of carbon deposits.

The research on low-coking and more stable catalytic systems for DRM currently focuses on the use of nickel-containing materials, since nickel shows a catalytic activity comparable to noble metals, but is cheaper and more abundant than the former ones [9–11]. On the contrary, nickel-based catalysts do not show acceptable stability in DRM due to the simultaneous promotion of concomitant C-forming side reactions. It has been lately reported that the stability of Ni-based catalyst in DRM is dependent on reaction conditions, the type of support, the interaction between the metallic nickel phase and the support, as well as on nickel particle size [6,12]. For example, the C-forming reactions (CH_4 decomposition, Boudouard reaction) occur more easily on large Ni crystallites which are normally formed upon highly endothermic DRM through the sintering of active phase [10]. Therefore one of the main strategies envisaged in the aim of increasing catalyst stability is decreasing Ni crystal size. This may be achieved through the utilisation of an appropriate support, able to properly disperse Ni-species, and/or to the presence of promoters. In general, the use of magnesia and alumina supports has shown to positively influence catalyst stability, by means of increasing their interaction with nickel species. This stronger interaction has been explained in terms of the formation of a NiO-MgO solid solution or $NiAl_2O_4$ spinel phase [13,14].

All required catalyst components i.e. Ni, magnesia and alumina may be introduced into one structure of hydrotalcite (layered dou-

* Corresponding author at: AGH University of Science and Technology, Faculty of Energy and Fuels, 30 A. Mickiewicza Avenue, 30-059, Kraków, Poland.
E-mail addresses: debek@agh.edu.pl, raddebek@gmail.com (R. Dębek).

http://dx.doi.org/10.1016/j.apcatb.2017.06.024
0926-3373/

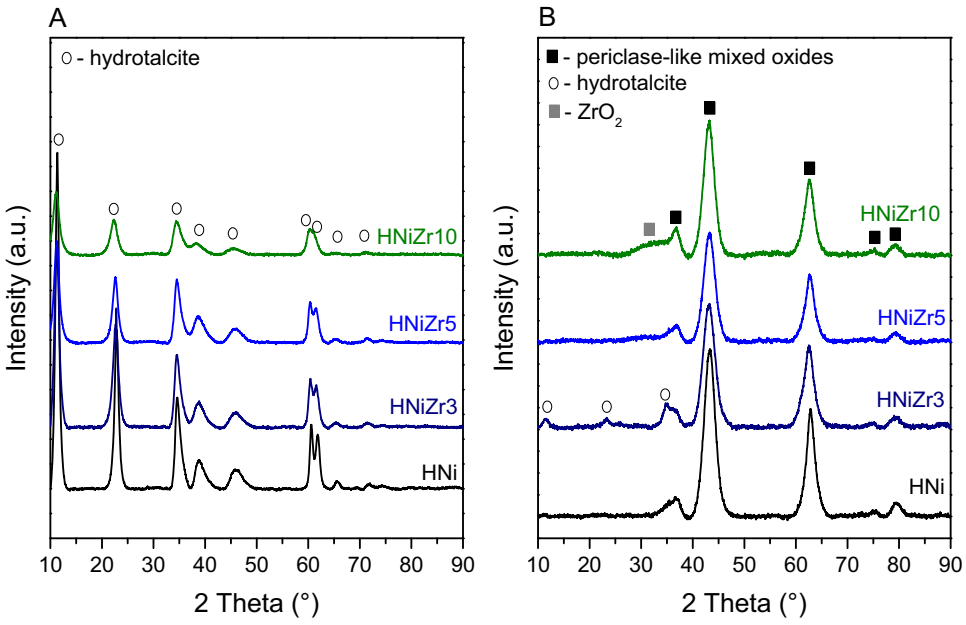

Fig. 1. XRD patterns of fresh hydrotalcites (A) and their thermal decomposition products (B).

ble hydroxide, HTs). Hydrotalcites are layered synthetic minerals, which can host various type of di-, tri- or even tetravalent cations in the brucite-like layers [15–17]. The spaces between layers are filled with charge compensating anions and water molecules. In consequence, the general formula of HTs may be expressed as $[M^{2+}_{1-x}M^{3+}_{x}(OH)_2][(A^{n-}_{x/n})\,mH_2O]$, where: M^{2+}, M^{3+} – di- and trivalent cations, A – interlayer anions, x – mole fraction of trivalent cations. The part $[M^{2+}_{1-x}M^{3+}_{x}(OH)]_2$ describes the composition of brucite-like layers whereas the part $[(A^{n-}_{x/n})\,mH_2O]$ describes composition of interlayer spaces.

Upon thermal treatment of HTs materials, their layer structure collapses and a homogenous mixture of nanooxides with periclase-like structure is formed. Such periclase-like oxides might be transformed into stable spinel phase upon further thermal treatment [18,19]. Additionally, HTs-derived materials possess basic properties and therefore promote CO_2 adsorption, what is thought to be beneficial for the DRM reaction [20–22]. Several studies already point to hydrotalcite-derived materials as prospective catalysts for DRM and other catalytic applications [23–28].

In our previous work we already considered nickel-containing hydrotalcite-derived catalytic systems for DRM, which turned out to be very promising catalysts [29–31]. Our latest study revealed that the addition of zirconium species (ca. 3 wt.%) into the hydrotalcite brucite layers resulted in a significant promotion of catalyst stability by means of the formation of smaller Ni particles which inhibited carbon-forming reactions, i.e. CH_4 decomposition [32]. In the present study we are aiming to carefully evaluate the influence of zirconia content in the Ni crystal size obtained upon the reduction of the hydrotalcite derived catalyst as well as its consequence in the overall performance of these Zr-promoted catalysts in CO_2 methane reforming.

2. Experimental

2.1. Catalysts preparation

Catalysts precursors (hydrotalcite materials) were prepared through a coprecipitation method at constant pH equal to 10 ± 0.2. An aqueous mixture of the appropriate Ni, Mg, Al and Zr nitrates (Sigma Aldrich) and a 1 M NaOH (POCH) solutions were prepared and subsequently added dropwise to a 0.05 M Na_2CO_3 solution at

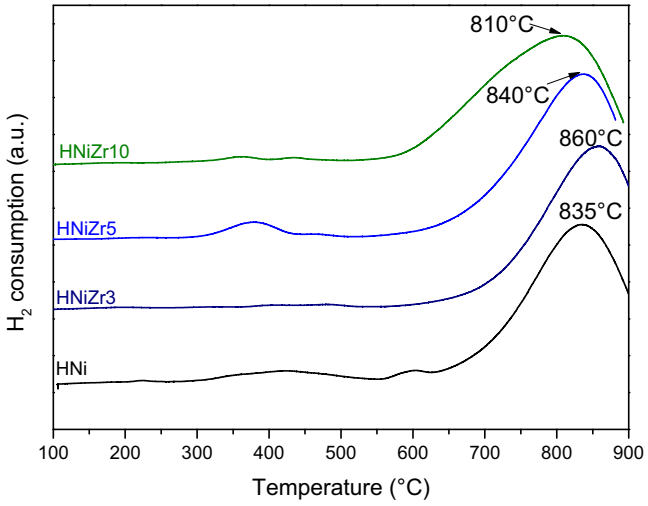

Fig. 2. H_2-TPR profiles recorded for various Zr-promoted hydrotalcite-derived catalysts.

65 °C. The obtained mineral suspension was maintained under vigorous stirring for 3 h at 60 °C, then filtered and dried overnight at 80 °C. Three hydrotalcite-like materials with Ni, Mg, Al and Zr species introduced into brucite-like layers were obtained. The content of Zr species was described by nominal value of Al/Zr molar ratio in brucite-like layers and was equal to 9:1, 8:2 and 6:4, respectively for samples denoted HNiZr3, HNiZr5 and HNiZr10. The molar ratio of divalent to tri- and tetra-valent cations was fixed to a value of 3 and kept equal for all the hydrotalcite precursors. Additionally, a non-promoted reference catalyst (composed of only Mg, Al and Ni species) was synthesized (sample HNi), following the same procedure. The so prepared HTs-like materials were calcined at 550 °C for 4 h. The calcination temperature of 550 °C was found to be enough to completely transform layered structure to nano mixed-oxides, as reported for hydrotalcites with various compositions [29,33].

2.2. Physiochemical characterization

The elemental composition of the catalysts was determined by means of X-ray fluorescence (XRF). These measurements were carried out in an energy dispersive XEPOS spectrometer from Spectro Ametek. X-ray diffraction (XRD) patterns were recorded in a 2θ range from 5 to 90° in an Empyrean diffractometer from PANalytical, equipped with a CuKα radiation source (λ = 0.154059 nm). Based on the diffractograms recorded for the reduced and for the spent catalysts, i.e. after DRM tests, the Ni crystal sizes were estimated, using the Scherrer equation. The reducibility of the catalyst was evaluated by means Temperature Programmed Reduction in H_2 (H_2-TPR) on BELCAT-M apparatus from BEL Japan, equipped with thermal conductivity detector. 50 mg of samples were degassed at 100 °C for 2 h. The samples were subsequently reduced in 5% (vol/vol) H_2/Ar between 100 and 900 °C at 7.5 °C/min heating rate. The same apparatus was used to evaluate the basicity of the catalysts through Temperature Programmed Desorption of CO_2 (CO_2-TPD) performed on previously reduced samples. The materials were first degassed for 2 h at 500 °C and then cooled to 80 °C. A mixture of 10% (vol/vol) CO_2/He was then introduced for 1 h in order to adsorb CO_2. A flow of He was subsequently fed for 15 min to desorb weakly physically adsorbed CO_2. The samples were further heated up to 800 °C under He flow at heating rate 10 °C/min, while the evolution of CO_2 was measured with the aid of TC detector. Scanning electron microscopy (SEM) analysis was carried out with the aid of JEOL JSM-7500F microscope coupled with INCAPentaFetx3 EDS system. The secondary electron detector provided SEM images and back-scattered electron detector provided BSE(COMPO) micrographs. The samples were coated with 20 nm Cr layer. Recorded SEM images allowed to study morphology of the calcined and reduced materials, as well as the catalysts after DRM reaction. The EDS analysis was used to check homogeneity of the tested materials. The catalysts before and after the DRM reaction were examined by Transmission Electron Microscopy (TEM, JOEL JEM-100CXII, acceleration voltage of 100 keV). Based on the analysis of the obtained images, the distribution of nickel crystallite size was discussed. The analysis of particle size distribution involved the analysis of at least 300 Ni crystals. The measurements of Ni particle size were performed using ImageJ software. Carbon formation during the DRM reaction was quantified using thermogravimetric analysis under air atmosphere. The experiments were carried out with a SDT Q600 apparatus (TA Instruments), under air flow of 100 cm^3/min with heating from ambient temperature to 900 °C at a rate of 10 °C/min.

2.3. CO_2 methane reforming (DRM) experiments

The behaviour of the studied catalysts in methane dry reforming was evaluated in a quartz fixed-bed reactor. A mixture of gases (CH_4/CO_2/Ar = 1/1/8) was fed into U-shape reactor. The total flow was equal to 100 cm^3/min and was adjusted with the aid of several mass flow controllers (BROOKS). The catalyst bed was supported on quartz wool. The mass of the catalyst was chosen so to work with constant value of gas hourly space velocity (GHSV) equal to 20 000 h^{-1}, which is commonly used in DRM catalytic tests on laboratory scale [34–36]. The reactor was placed inside an electrically heated furnace. Temperature in this oven and inside the catalytic bed was controlled with the aid of different thermocouples and a temperature controller. The gaseous products of DRM reaction were passed through a water trap and subsequently analyzed in a CPi 490 Varian micro gas chromatograph equipped with COX column and a thermal conductivity detector. Prior to each catalytic test, material was reduced in-situ in a stream of 5%H_2 in Ar at 900 °C for 1 h. Catalyst bed was subsequently washed with Ar and cooled down to the desired reaction temperature (550, 650 or 750 °C).

Additionally, the catalytic activity towards direct CH_4 decomposition was investigated using the same catalytic setup. The reaction conditions were kept constant while the feed gas composition was changed to a CH_4-containing gas of CH_4/Ar molar ratio equal to 2/8.

The conversions of CH_4 and CO_2, the product yield, given as H_2/CO molar ratio, as well as the carbon balance, during both DRM and methane decomposition reaction, were calculated using the following equations:

$$\%CH_4 conversion = \frac{F_{CH_4,in} - F_{CH_4,out}}{F_{CH_4,in}} \cdot 100\% \quad (2)$$

$$\%CO_2 conversion = \frac{F_{CO_2,in} - F_{CO_2,out}}{F_{CO_2,in}} \cdot 100\% \quad (3)$$

$$\frac{H_2}{CO} molar ratio = \frac{F_{H_2,out}}{F_{CO,out}} \quad (4)$$

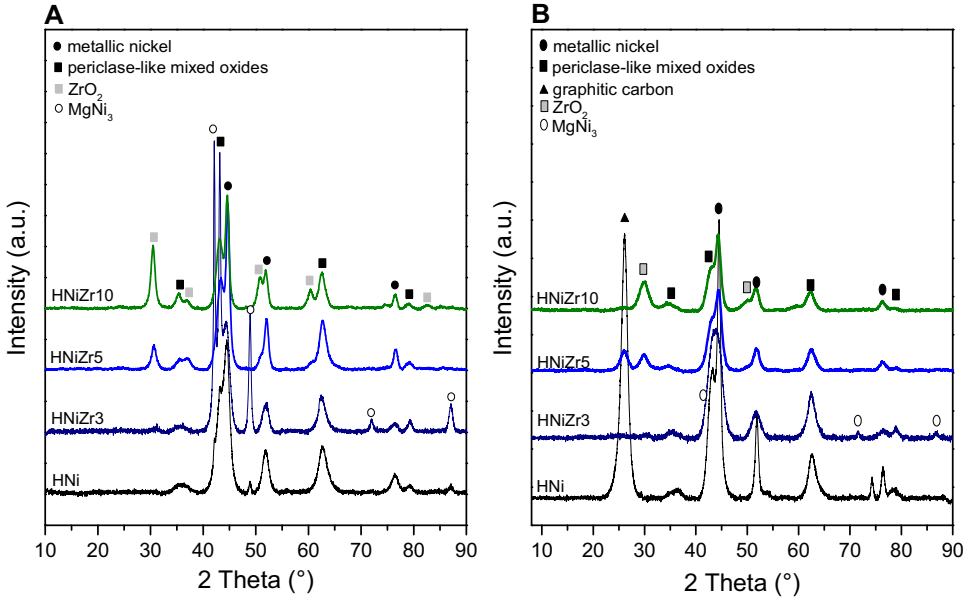

Fig. 3. XRD diffractograms recorded for reduced catalysts (A) and spent samples after 5 h DRM catalytic tests at 550 °C (B).

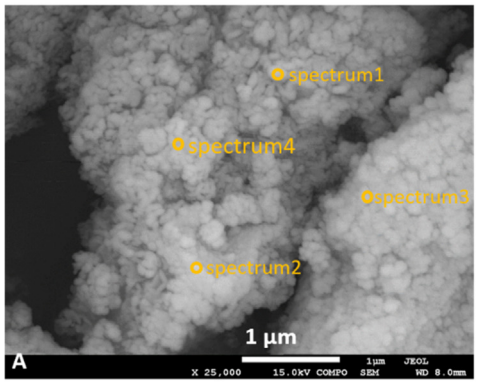

Spectrum	Mg	Al	Ni
Spectrum1	17.7	7.6	4.4
Spectrum2	16.1	6.8	4.1
Spectrum3	17.1	7.2	4.2
Spectrum4	17.2	8.1	5.7
Mean	17.0	7.4	4.6

All results in weight %

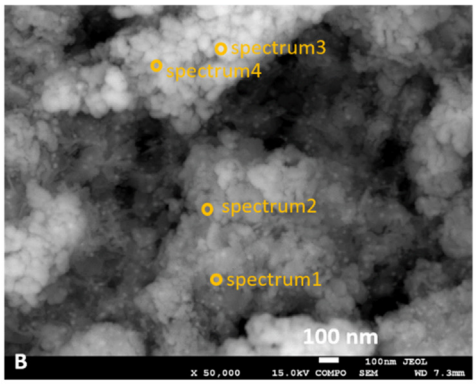

Spectrum	Mg	Al	Ni	Zr
Spectrum1	20.2	8.4	7.7	0.6
Spectrum2	20.3	8.3	8.0	0.6
Spectrum3	18.6	7.6	5.9	0.8
Spectrum4	18.8	8.0	6.7	0.5
Mean	19.5	8.1	7.1	0.6

All results in weight %

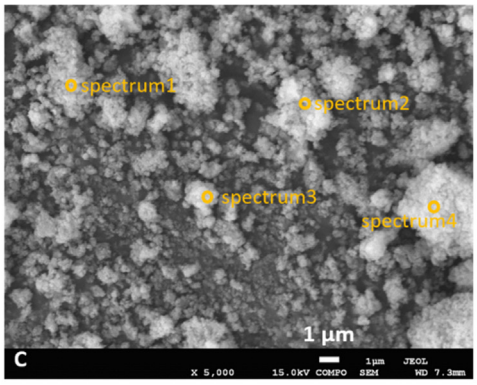

Spectrum	Mg	Al	Ni	Zr
Spectrum1	53.6	23.9	18.9	3.5
Spectrum2	55.6	21.6	19.2	3.6
Spectrum3	53.1	23.2	19.2	4.4
Spectrum4	55.0	24.2	15.8	5.0
Mean	54.3	23.2	18.3	4.1

All results in weight %

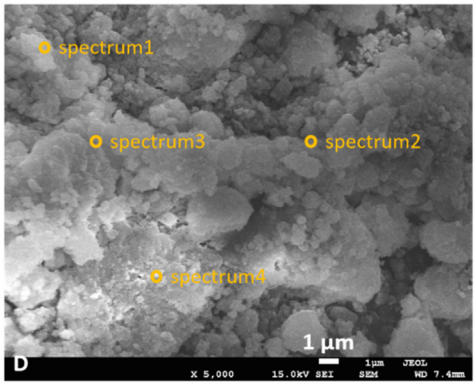

Spectrum	Mg	Al	Ni	Zr
Spectrum1	53.7	15.8	20.3	10.2
Spectrum2	56.1	21.0	15.1	7.8
Spectrum3	58.2	17.5	18.6	5.7
Spectrum4	51.5	17.4	21.3	9.8
Mean	54.9	17.9	18.8	8.4

All results in weight %

Fig. 4. SEM micrographs and results of EDX analysis performed for reduced catalysts: (A) HNi (×25000), (B) HNiZr3 (×50000), (C) HNiZr5 (×5000) and (D) HNiZr10 (×5000).

$$\%Cbalance = \frac{F_{CH_{4,out}} + F_{CO_{2,out}} + F_{CO_{out}}}{F_{CH_{4,in}} + F_{CO_{2,in}}} \cdot 100\% \quad (5)$$

where $F_{in/out}$ corresponds to the flow rate of each component in the feed or effluent.

3. Results and discussion

3.1. Physicochemical features of catalyst precursors

The XRD diffractograms recorded for freshly prepared hydrotalcites (HTs), as well as for the calcined materials are contained in Fig. 1. Fresh hydrotalcites exhibit several reflections at 2θ equal to

Table 1
Unit cell parameters of freshly synthesized hydrotalcites.

Sample	Unit cell parameter (Å)		
	a	*c*	*c'* = *c*/3
HNi	3.056	23.39	7.80
HNiZr3	3.068	23.55	7.85
HNiZr5	3.069	23.63	7.88
HNiZr10	3.076	23.84	7.95

ca. 11, 22 and 35°, characteristic of the layered structure of HTs-like materials [16,18] (ICOD 00-022-0700). The intensity of these reflections decreases with increasing Zr content, pointing to a loss in crystallinity as a consequence of the increasing presence of this Zr^{4+} cation. No additional reflections are observed, what points to a successful incorporation of Ni and Zr species into HT brucite layers. Following the procedure described by Rives et al. [18], the unit cell parameters *a* and *c* were calculated (Table 1). Unit cell parameter *a*, which describes average cation–cation distances in HT brucite-like layers, increases with increasing Zr content. As Zr^{4+} (0.072 nm) has a larger ionic radii than Al^{3+} (0.053 nm), substitution of Al^{3+} by Zr^{4+} expectedly increases the value of lattice parameter *a*, as has been moreover previously described in literature [37,38]. The values of unit cell parameter *c* were in the range 23.39-23.85 Å and also increased with increasing Zr content. Since the value of this parameter is dependent on the type of anions present between HT layers, this points to the presence of different of interlayer species, maybe carbonates, whose presence is moreover related to the presence and increasing content of Zr.

Upon calcination, the layered hydrotalcite structure was transformed into an homogenous mixture of nano-oxides having a periclase-like structure (Fig. 1B), as confirmed by the presence of the reflections at 2θ at ca. 37, 43, 62, 75 and 75° (ICOD 00-004-0829). The diffractogram obtained for the calcined catalyst containing the lowest amount of Zr still presents several reflections corresponding to the pristine hydrotalcite structure. This indicates that the incorporation of small amounts of Zr into the brucite layers stabilizes the hydrotalcite structure (rhombohedral), and thus higher calcination temperatures are required in order to complete its transformation into a periclase mixed oxides phase (cubic). With the increase of Zr content, a small intensity reflection was observed at 2θ ca. 32°, pointing to the formation of a segregated zirconia phase (ICOD 01-083-0810).

The results of the elemental analysis (XRF) are summarized in Table 2. The materials presented Ni contents within 16–20 wt.%, in good agreement with the targeted nominal values. The catalysts HZrNi3, HZrNi5 and HZrNi10 respectively contained 2.5, 5.4 and 9.7 wt.% of Zr upon calcination. Note here that the nominal Al/Zr ratios are all the time lower than the experimentally determined ones. This may point to an apparent loss of Zr to another oxide phase, most probably a mixed oxide phase, in which Mg and Ni-species would be as well involved. Due to the small amount of Zr added, it is impossible to distinguish this mixed oxide phase in the XRD profiles (Fig. 1).

Table 3 presents the textural parameters calculated from the N_2 sorption isotherms obtained for the calcined hydrotalcite derived materials. The values of specific surface area range between 110 and 254 m^2/g, in good agreement with the values previously reported in literature for this kind of materials [16,39,40]. The addition of Zr results in an increase of the specific surface area. This is particularly remarkable in the case of the catalyst containing 2.5 wt.% of Zr (HNiZr3). This increase is accompanied by an increase in total pore volume and, at the same time, by a substantial decrease of the average pore sizes, i.e. 3 nm for HNiZr3 vis-à-vis 14 nm measured in the non-promoted HNi catalysts. As Zr content increases, a separated ZrO_2 phase appears, as evidenced in the XRD patterns acquired for these materials. The formation of this segregated phase leads to slight pore blockage for HZrNi5 and HZrNi10.

Table 3
Textural parameters (specific surface area, total pore volume and mean pore diameter) and total basicity determined for the prepared materials.

Sample	S_{BET} (m^2/g)	V_{tot} (cm^3/g)	d_r (nm)	Total basicity[a]	
				(μmol/g)	(μmol/m^2)
HNiZr3	254	0.62	3	38	0.150
HNiZr5	198	0.32	6	61	0.310
HNiZr10	152	0.34	6	160	1.053
HNi	115	0.41	14	105	0.913

S_{BET} – Specific Surface Area; V_{tot} – Total volume of pores; d_r –mean pore diameter.
[a] measured for reduced catalysts by CO_2-TPD.

3.2. Reducibility of Ni species and acid-base properties

Fig. 2 contains the H_2-TPR profiles registered for the calcined hydrotalcite derived catalysts. All of them present one asymmetric reduction peak centered between 600 and 900 °C, which correspond to the reduction of strongly bonded Ni species inserted within the lattice of periclase mixed oxide structure. Additional smaller intensity reduction peaks are also observed at temperatures within 400–600 °C. They are related to the reduction of NiO in weak interaction with the support, as reported in [41–43]. In the case of hydrotalcite derived catalysts, their presence may be related to a part of NiO that segregated from the mixed oxide structure. The addition of Zr influences the reducibility of Ni-species. Moreover, this effect is dependent on Zr content. The addition of 2.5 wt.% of Zr into the brucite-like layers decreases the reducibility of Ni-species with respect to the unpromoted catalyst. This decrease in reducibility becomes less noticeable with increasing Zr loading, i.e. for HNiZr5, and for HNiZr10 a slight increase in reducibility can be even observed. When Zr is present together with Ni in the Mg(Al,Ni,Zr)O lattice, the strong interaction of Ni cations in this mixed oxide structure results in decreased reducibility. On the contrary, the presence of segregated Zr-species outside the periclase structure, i.e. ZrO_2, facilitates the reduction of Ni-species. These results stay in line with the size of Ni crystallites estimated applying the Scherrer to the XRD diffractograms recorded for each reduced samples (results presented in Table 4). The addition of 2.5 wt.% Zr does not remarkably affect Ni particle size, which, in spite of decreased reducibility, remains very similar for both HNiZr3 and the unpromoted HNi catalyst. Higher Zr loadings, accompanied by the formation of segregated zirconia phase, result in the formation of larger Ni crystallites, i.e. 9 and 10 nm respectively for HNiZr5 and HNiZr10.

Table 2
Elemental composition of the prepared materials determined by XRF.

Sample	Ni (wt.%)	Mg(wt.%)	Al (wt.%)	Zr (wt.%)	Ni/Mg[a]	Al/Zr[a]
HNiZr3	17.3	24.0	9.7	2.5	0.30 (0.33)	13.0 (9)
HNiZr5	18.9	25.2	8.9	5.4	0.31 (0.33)	5.5 (4)
HNiZr10	16.3	18.2	4.7	9.7	0.37 (0.33)	1.6 (1.5)
HNi	19.6	23.9	11.8	–	0.34 (0.33)	–

[a] molar ratio; in the parenthesis nominal values are given.

Table 4
Ni crystallites calculated for the reduced and spent catalysts after DRM, coke deposition determined by TG and carbon balance during DRM catalytic tests at 550 °C.

Sample	Ni crystallite size[a] (nm)		Deposited coke[b] ($g/h\,g_{cat}$)	Weight loss[b] (%)	Carbon balance (%)	
	Reduced sample	Sample after DRM			at TOS 1h	at TOS 5h
HNiZr3	6	3	0.03	12.7	97.0	99.7
HNiZr5	9	9	0.14	40.7	94.7	94.3
HNiZr10	10	10	0.16	43.7	93.3	92
HNi	6	11	0.22	52.7	90.9	84.7

[a] estimated by Scherrer equation.
[b] determined by TG experiments.

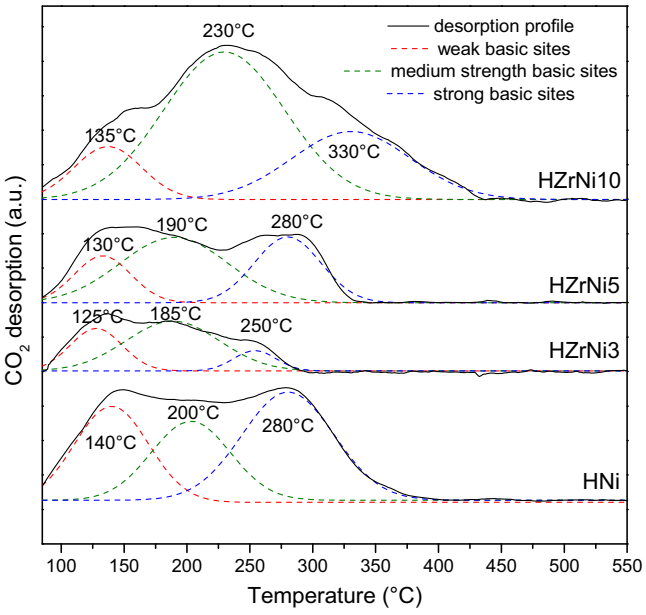

Fig. 5. CO_2-TPD profiles registered for reduced catalysts.

The presence of Zr further influences structure and the phase composition of the reduced catalysts, as confirmed by XRD (Fig. 3B). The diffraction peaks characteristic of metallic nickel (2θ: 44.5, 51.8, 76; ICOD 01-087-0712) and Mg(Ni,Al)O nano mixed oxides (periclase structure, 2θ: 43, 62.5° ICOD 00-045-0946) are observed for all the reduced catalysts. Small reflections originating from tetragonal zirconia (2θ: 30, 35, 50, 60; ICOD 01-080-2156) can be observed in all Zr-promoted materials. The intensity of these reflections increases with increasing Zr content. An additional phase is evidenced in the pattern acquired for the reduced HNiZr3 catalyst, corresponding to $MgNi_3$ (2θ: 42, 49, 72, 87; ICOD 04-016-6336). The presence of this $MgNi_3$ points to a further enhanced interaction between Mg and Ni oxides in this case.

The SEM micrographs acquired for the reduced catalysts are shown in Fig. 4. The Zr-promoted materials exhibit very similar morphologies than the unpromoted catalyst. The absence of important morphological changes upon Zr addition points to very high dispersion of tiny zirconia aggregates (especially for HNiZr5 and HNiZr10 samples) in the bulk and on the surface of the catalysts. The results of EDX analysis, performed in various zones of the reduced materials, evidenced uniform composition for all the prepared catalysts.

As already reported in literature [29,30,44,45], the total basicity of hydrotalcite-derived materials, as well as the distribution of weak, intermediate and strong basic sites, is strongly dependent on the HTs composition, and greatly influences catalytic performance in DRM. The basicity of the reduced HNiZr3, HNiZr5, HNiZr10 and HNi catalysts was investigated by means of CO_2-TPD experiments, the results are presented in Fig. 5 and Table 3. Typically, HTs-derived materials exhibit three types of basic sites [21,30,45]: (i) weak basic sites associated with Brønsted hydroxyl groups (desorption peak centered at ca 130 °C), (ii) intermediate strength basic sites associated with Lewis acid-base, metal-oxygen pairs (desorption peak centered at ca. 190 °C) and (iii) strong basic sites related to low coordinated O^{2-} anions (desorption peak centered at ca. 280 °C). The Zr loading, and thus presence of Zr species either in the framework of periclase-like mixed oxides or as a separate phase, influence both total basicity and the distribution of weak, medium and strong basic sites (Fig. 5). The catalyst HNiZr3 shows the lowest total basicity, while HNiZr5 and HNiZr10 catalysts exhibit a significant increase in the total basicity, especially in terms of intermediate and strong basic sites, vis-à-vis HNiZr3. Moreover, a shift

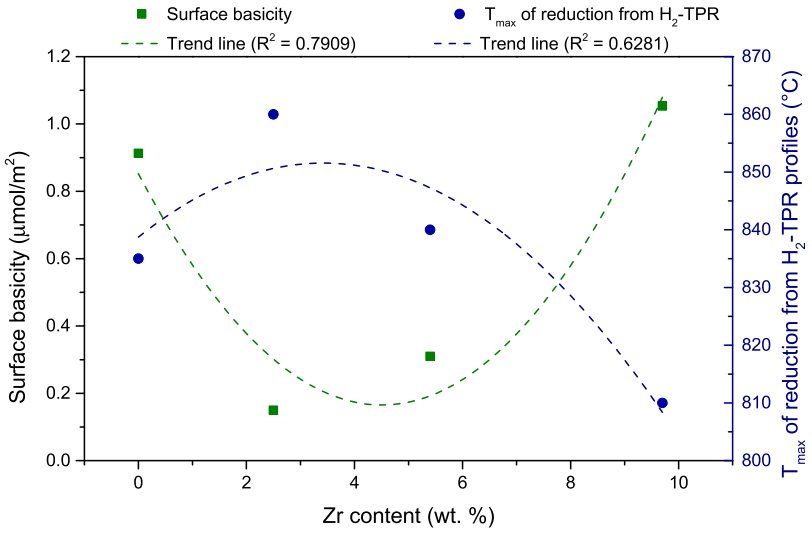

Fig. 6. Correlation between Zr content, surface basicity and reducibility of catalysts.

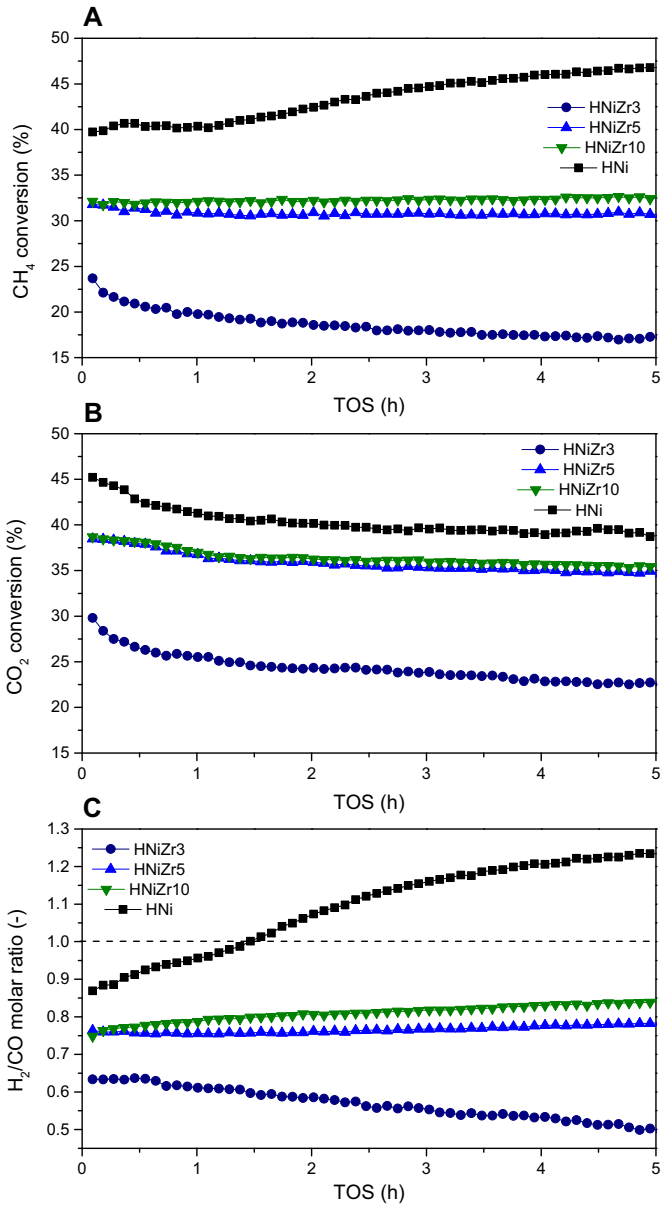

Fig. 7. Results of DRM catalytic tests: (A) CH_4 conversion, (B) CO_2 conversion, (C) H_2/CO molar ratio; Temperature 550 °C, $CH_4/CO_2/Ar = 1/1/8$; GHSV = 20000 h^{-1}; total flow 100 cm^3/min;.

towards higher CO_2 desorption temperatures can be observed with increasing Zr content. This can be attributed to the presence of a separate ZrO_2 phase on the reduced HNiZr5 and HNiZr10, offering new and strong or medium-strength basic sites.

Total surface basicity (Table 3) increases with the increasing Zr content. When correlated to the reducibility of Ni-species, i.e. H_2-TPR profiles (Fig. 6), it can be clearly observed that this minimal surface basicity corresponds to the highest peak reduction temperatures in these profiles, occurring at about 2.5–4.5 wt.% Zr content. This fact therefore reveals that there is a relationship between Zr content, surface basicity and the reducibility of Ni species. It is not straightforward to establish a link between the segregation of Zr species, implying the formation of a mixed oxide phase, and total surface basicity, since other species, including reduced Ni, may as well contribute to CO_2-TPD profiles. Total surface basicity and Ni reducibility seem to be related to Zr content, as stated before, pointing therefore to an indirect link between Zr segregation and surface basicity.

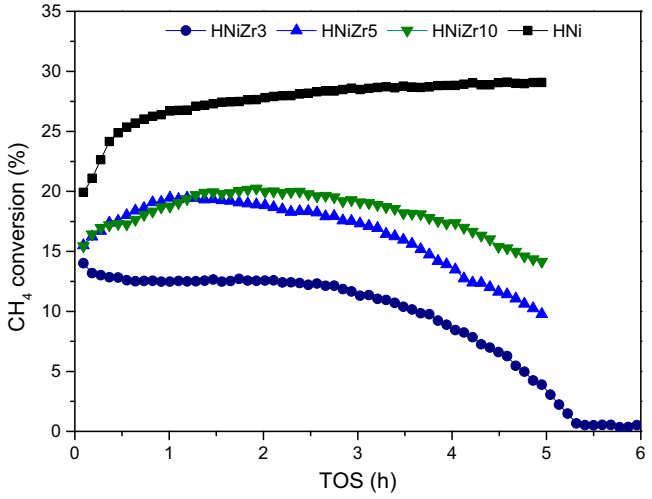

Fig. 8. Results of direct CH_4 decomposition experiments carried out over different HT-derived catalysts at 550 °C; $CH_4/Ar = 2/8$; GHSV = 20000 h^{-1}; total flow 100 cm^3/min.

3.3. Activity and selectivity in low temperature DRM

The catalytic activity of Zr-promoted HT-derived catalysts in DRM was investigated in a first series of tests at 550 °C (Fig. 7). Promotion by Zr results in decreased catalytic activity with CH_4 and CO_2 conversions following the sequence: HNi > HNiZr10 ≈ HNiZr5 > HNiZr3. Among the Zr-promoted catalysts, the catalytic activity decreases with decreasing Zr loading. The catalysts HNiZr5 and HNiZr10 show very similar performance, especially towards CO_2 conversion. The enhanced reducibility of Ni-species in these two materials may be responsible of their better performance. Moreover, reverse water gas shift can be promoted in the presence of segregated ZrO_2 sites of strong basic character. In all cases, a decrease of CO_2 conversion with time-on-stream (TOS) can be observed, more evident for HNi and HNiZr3, and corresponding to ca. 6 and 7% activity loss, respectively. At the same time, the unpromoted catalyst, HNi, and the Zr-promoted HNiZr5 and HNiZr10 catalysts, show an increase in CH_4 conversion with time on stream, pointing to a further evolution of Ni-species with TOS.

As already stated, Zr-promotion drastically changes the selectivity of the process. The Zr-promoted catalysts exhibit higher conversions of CO_2 than those of CH_4 (Fig. 7A and B), this being accompanied by an excess of CO in the products of the reaction (Fig. 7C). This effectively points to the occurrence of reverse water gas shift (RWGS). The opposite is observed for the unpromoted catalysts (excess of H_2, higher conversions of CH_4 than CO_2). In our previous work, we reported increasing conversion of CH_4 with TOS for unpromoted Ni/Mg/Al catalyst with Ni loading in the range 12–60 wt.%, and attributed it to the increasing occurrence of direct CH_4 decomposition, resulting in the formation of the carbon deposits [29], while Zr-promotion using 3 wt% resulted in the inhibition of this important side reaction [32].

The results of the CH_4 decomposition experiments performed at 550 °C in the presence of this series of catalysts are shown in Fig. 8. Methane conversion is higher for the non-promoted HNi catalysts and once again increases with TOS. For the Zr-promoted catalysts a decrease of CH_4 conversion with decreasing Zr loading can be observed. The catalysts HNiZr5 and HNiZr10 present very similar activity during first the hours TOS, which may explain their similar performance in DRM. The most interesting results are obtained for the HNiZr3 catalyst, which completely inhibits direct CH_4 decomposition after ca. 5,5 h TOS. Moreover, the catalysts HNiZr5 and HNiZr10 also show a decrease in activity after approximately 1.5 h

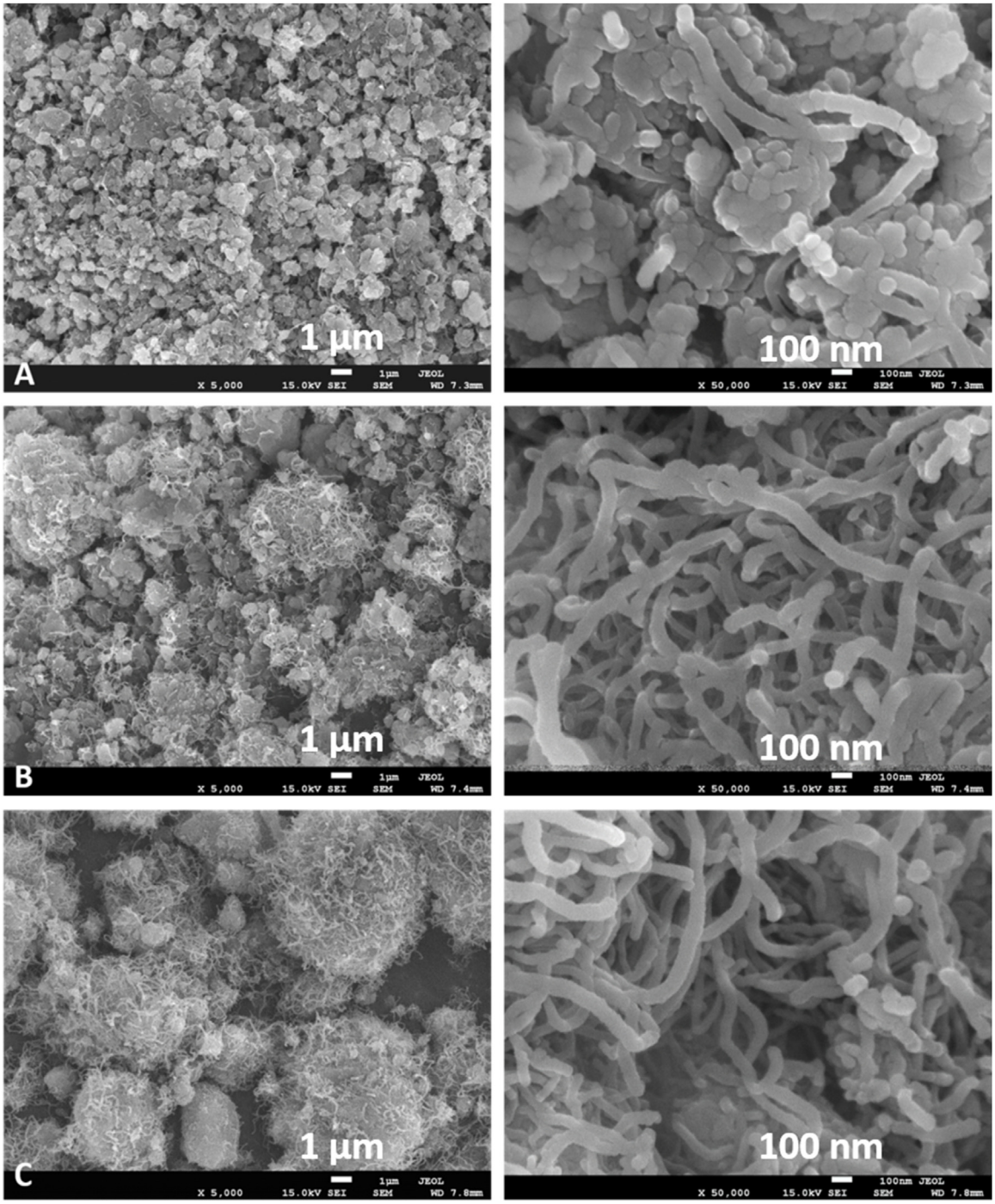

Fig. 9. SEM images registered for the Zr-promoted catalysts after 5 h TOS DRM catalytic tests: (A) HNiZr3, (B) HNiZr5 and (C) HNiZr10; first column magnification ×5000, second column magnification ×50000.

TOS, pointing to an evolution of surface properties resulting as well in the inhibition of this parallel side reaction. Zr promotion is however dependent on the presence of Zr species either as a separate phase or in the framework of Mg(Ni,Al,Zr)O mixed-oxides, which may be controlled to a certain extent by controlling Zr loading.

3.4. *Influence of Zr content on catalyst stability: carbon formation*

With the aim of gaining insight into the type and amount of the carbon deposits formed upon reaction, the spent catalysts obtained after the 5 h TOS experiments under DRM conditions were analysed by means of temperature controlled thermogravimetric oxidation (Table 4) and XRD (Fig. 3B, Table 4). The total amount of carbon deposited determined in the thermogravimetric experiments follows the same trend than the catalytic activity in DRM and direct CH_4 decomposition determined for the different catalysts, i.e. higher C amount was formed and deposited on the HNi unpromoted catalysts, pointing to a positive effect Zr-promotion in terms of catalytic stability.

The XRD diffractograms obtained for the spent catalysts (Fig. 3 B) further confirms that Zr-promotion inhibits C-formation. The high intensity diffraction peak at about 26° 2θ appearing in the pattern for the spent HNi catalyst directly point to the formation of graphitic carbon (ICOD 01-075-1621). Such reflection can

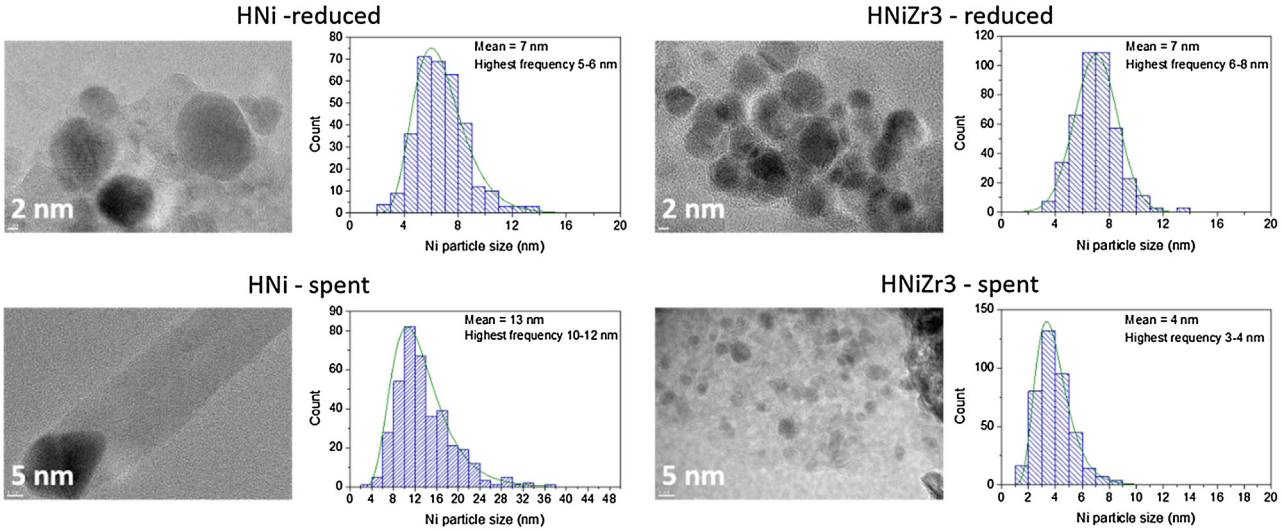

Fig. 10. TEM images and corresponding distribution of nickel particles registered for the spent catalysts (HNi and HNiZr3) after 5 h DRM reaction at 550 °C.

be also slightly observed in the pattern acquired for HZrNi5 and becomes practicable negligible for HZrNi10 and HZrNi3. Moreover, The examination of the surface of the spent catalysts using scanning electron microscopy (SEM, Fig. 9) evidenced important changes in morphology occurring after the DRM reaction. Whisker-like carbon filaments having diameters around 40–90 nm are clearly visible in the SEM micrographs acquired. Moreover, the amount and diameter of these carbon fibres increases with increasing Zr loading.

The activity of DRM nickel-based catalysts towards C-forming side reactions is notably influenced by Ni crystallite size. Large Ni crystals promote direct methane decomposition and Boudouard reaction [10]. As reported by Kim et al. [46], who investigated Ni/γ-Al_2O_3 systems in DRM, the minimal size of nickel crystallites needed for the formation of whisker-like carbon deposits is 7 nm. The Ni crystallite size calculated from the XRD patterns obtained for the reduced and spent catalysts (Table 4) evidences an important sintering of Ni particles upon reaction in the case of the non-promoted catalyst, HNi, i.e. Ni crystal size increasing from 6 to 11 nm, which explains higher formation of carbon deposits and the increasing CH_4 conversion upon DRM catalytic tests. No evidence of sintering is found for the catalysts HNiZr5 and HNiZr10. However, the Ni particle sizes estimated are still large enough to promote coking. Interestingly, a decrease in Ni crystal size upon DRM reaction is observed for HNiZr3 catalyst, i.e. varying from 6 nm to 3 nm. These results were additionally confirmed by TEM analysis (Fig. 10). The presence of small Ni crystallites on the surface of HNiZr3 catalyst explain their low activity at 550 °C in comparison to other catalysts, but at the same time, it is a guarantee for stable performance and higher resistance to coking. At the same time the loss in crystallinity of zirconia phase was observed for HNiZr5 and HNiZr10 catalysts (e.g. estimated zirconia particle size decreased from ca. 8 nm to 5 nm respectively for reduced and spent HNiZr10 catalyst), indicating the redistribution of both nickel and zirconium species on the catalysts surface upon DRM reaction.

3.5. Activity in DRM at 550, 650 and 750 °C

The catalyst HNiZr3 exhibiting the highest coking resistance properties was selected for additional catalytic tests at elevated temperatures (650 and 750 °C). The results of these experiments are depicted in Fig. 11A–C. At 650 and 750 °C Zr-promoted sample shows more stable performance regarding activity towards both CH_4 and CO_2 than at 550 °C, since no significant decrease in the conversions was observed. The CO_2 and CH_4 conversions tend to converge with increasing temperature, what is also reflected in the increasing values of H_2/CO molar ratio.

The average values of H_2/CO molar ratio and CH_4 and CO_2 conversions registered during 5 h isothermal tests carried out over HNiZr3 and unpromoted HNi catalysts at 550, 650 and 750 °C are depicted in Fig. 11 D, E and F. The Zr-promoted catalyst exhibit conversions of CH_4 and CO_2 lower than HNi. However, the differences in activity between HNiZr3 and unpromoted catalyst decrease with the increasing reaction temperature. At 750 °C both samples showed similar CH_4 and CO_2 conversions, i.e. 83 and 90%, respectively, and H_2/CO molar ratios around 0.93. Both conversions increase with the increasing temperature, the latter reaching the thermodynamic equilibrium values at 650 and 750 °C.

The distribution of the obtained products (Fig. 11D) clearly shows that the Zr addition changed the catalyst selectivity towards DRM. HNiZr3 catalyst yields increasing values of H_2/CO ratios with increasing reaction temperature, indicating the influence of CO forming reactions, mainly RWGS, especially at low temperature. On the other hand, the unpromoted catalyst exhibits decreasing values of H_2/CO molar ratio with the increase in temperature, pointing to a more important H_2 production as a result of the concomitant occurrence of methane decomposition.

4. Conclusions

Zr-promoted hydrotalcite-derived catalysts were tested in the reaction of dry methane reforming. The effect of various Zr loadings on the catalytic properties was investigated. The Zr species (ca. 3, 5 and 10 wt.%) were introduced into hydrotalcite structure at the co-precipitation stage. The characterization of catalyst precursors confirmed the successful introduction of Zr species into HTs brucite-like layers. However, this species were derived from the framework of parental material upon calcination and H_2 activation for samples loaded with more than 3 wt.% Zr. The final catalysts contained zirconium species either in the framework of periclase-like mixed oxides or as a separate phase of zirconia, highly dispersed on the catalyst surface. The formation of various Zr-containing structures was influenced by Zr loading. The properties of the obtained samples. textural properties, reducibility of Ni species, materials basicity and thus their catalytic activity in DRM were dependent on the amount of introduced Zr and, as a consequence, also their placement in the catalytic systems. The position of Zr species in the

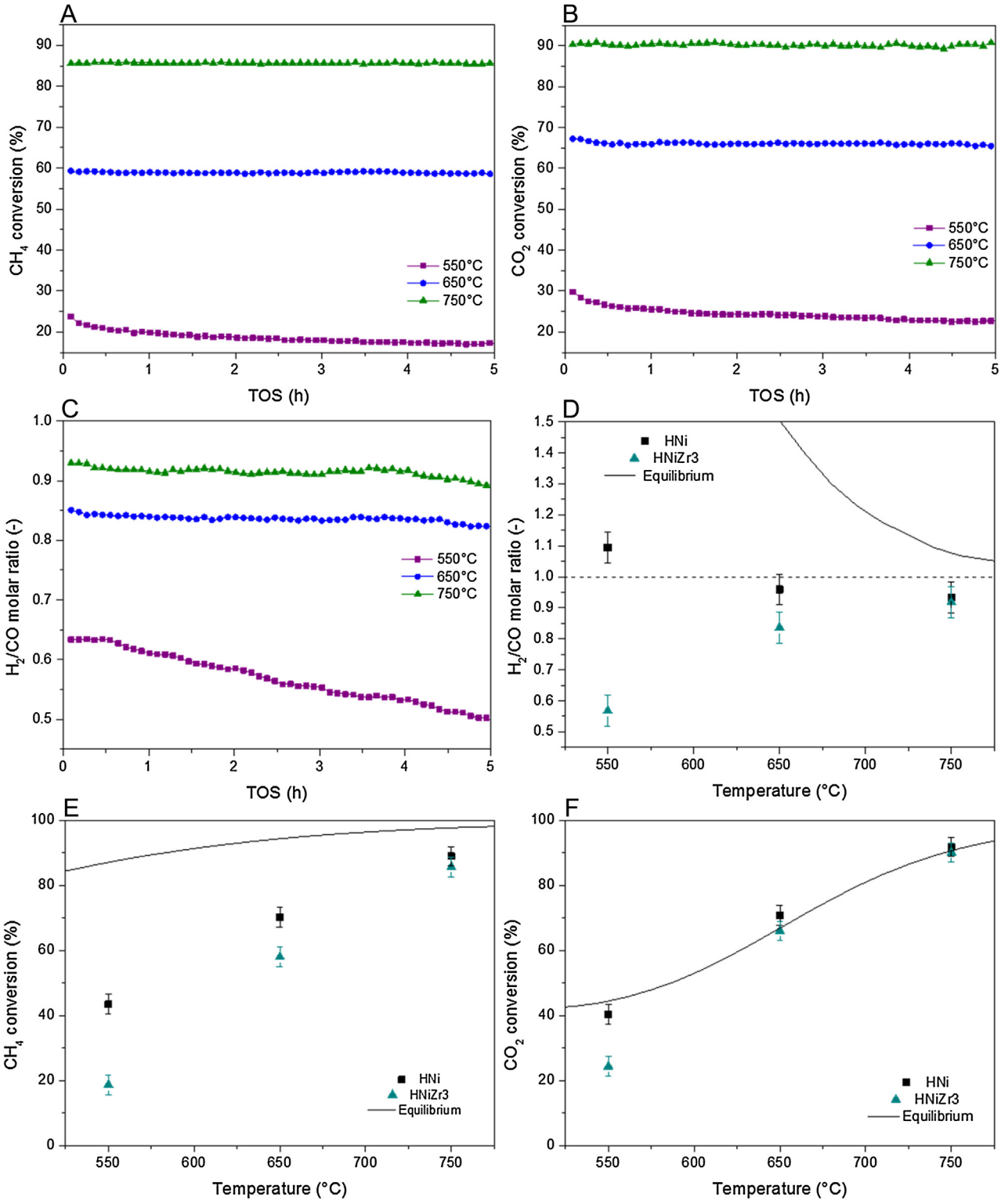

Fig. 11. Results of catalytic tests carried out over HNiZr3 catalyst: (A) CH_4 conversion, (B) CO_2 conversions and (C) H_2/CO molar ratio; and average values of H_2/CO molar ratio (D), CH_4 conversion (E) and CO_2 conversion (F) as a function of temperature registered at 550, 650 and 750 °C; $CH_4/CO_2/Ar = 1/1/8$; GHSV = 20000 h^{-1}; total flow 100 cm^3/min;.

framework of Mg(Ni,Al,Zr)O mixed oxides turned out to be important for improving catalyst resistance to coking by rearranging Ni crystallites into smaller aggregates upon DRM reaction at 550 °C. This effect needs to be further investigated in order to completely understand the synergetic effect between Ni and Zr species.

Catalytic tests carried out at 650 and 760 °C over HNiZr3 catalyst revealed that at elevated reaction temperatures competitive side reactions, such as CH_4 decomposition or Boudouard reaction, may influence the overall process stronger than at 550 °C, resulting in higher carbon deposition. However, no decrease in CH_4 and CO_2 conversions was observed and CO_2 conversions reached equilibrium values at the former.

Acknowledgments

The work was financed by AGH grant 11.11.210.213. R.Dębek would like to acknowledge for the financial support of the French Embassy in Poland and InnoEnergy PhD School.

References

[1] A.J. Hunt, E.H.K. Sin, R. Marriott, J.H. Clark, Generation, capture, and utilization of industrial carbon dioxide, ChemSusChem 3 (2010) 306–322.
[2] IPCC, Capture of CO_2, in: B. Metz, O. Davidson, H.C. de Conick, M. Loos, L.A. Meyer (Eds.), IPCC Special Repost on Carbon Dioxide Capture and Storage, Prepared by Working Group III of the Intergovernmental Panel on Climate Change, Cambridge, United Kingdom and New York, NY, USA, 2005, pp. 107–171, 2005.
[3] COM (2014) 15 final, Communication From The Commission To The European Parliament, The Council, The European Economic and Social Committee and The Committee of the Regions, A Policy Framework for Climate and Energy in the Periodfrom 2020 to 2030, European Commission, Brussels, 2014, pp. 1–18.
[4] European Commission, Energyroadmap 2050, Publications Office of the Eueopean Union, Belgium, Luxembourg, 2012.
[5] J.-M. Lavoie, Review on dry reforming of methane, a potentially more environmentally-friendly approach to the increasing natural gas exploitation, Front. Chem. 2 (2014).
[6] M. Usman, W.M.A. wan daud, H.F. Abbas, Dry reforming of methane: influence of process parameters—a review, Renew. Sustain. Energy Rev. 45 (2015) 710–744.
[7] M.S. Fan, A.Z. Abdullah, S. Bhatia, Catalytic technology for carbon dioxide reforming of methane to synthesis gas, ChemCatChem 1 (2009) 192–208.
[8] J.T. Richardson, S.A. Paripatyadar, Carbon dioxide reforming of methane with supported rhodium, Appl. Catal. 61 (1990) 293–309.
[9] H. Ay, D. Üner, Dry reforming of methane over CeO2 supported Ni, Co and Ni–Co catalysts, Appl. Catal. B Environ. 179 (2015) 128–138.
[10] Y.H. Hu, E. Ruckenstein, Catalytic conversion of methane to synthesis gas by partial oxidation and CO2 reforming, in: Advances in Catalysis, Academic Press, 2004, pp. 297–345.
[11] M.-S. Fan, A.Z. Abdullah, S. Bhatia, Utilization of greenhouse gases through dry reforming: screening of nickel-based bimetallic catalysts and kinetic studies, ChemSusChem 4 (2011) 1643–1653.
[12] J.H. Edwards, A.M. Maitra, The chemistry of methane reforming with carbon dioxide and its current and potential applications, Fuel Process. Technol. 42 (1995) 269–289.
[13] E. Baktash, P. Littlewood, R. Schomäcker, A. Thomas, P.C. Stair, Alumina coated nickel nanoparticles as a highly active catalyst for dry reforming of methane, Appl. Catal. B Environ. 179 (2015) 122–127.
[14] R. Zanganeh, M. Rezaei, A. Zamaniyan, Dry reforming of methane to synthesis gas on NiO–MgO nanocrystalline solid solution catalysts, Int. J. Hydrogen Energy 38 (2013) 3012–3018.
[15] S. Velu, K. Suzuki, M. Okazaki, T. Osaki, S. Tomura, F. Ohashi, Synthesis of new Sn-incorporated layered double hydroxides and their thermal evolution to mixed oxides, Chem. Mater. 11 (1999) 2163–2172.
[16] F. Cavani, F. Trifirò, A. Vaccari, Hydrotalcite-type anionic clays: preparation, properties and applications, Catal. Today 11 (1991) 173–301.
[17] C. Forano, U. Costantino, V. Prévot, C.T. Gueho, Chapter 14.1—layered double hydroxides (LDH), in: B. Faïza, L. Gerhard (Eds.), Developments in Clay Science, Elsevier, 2013, pp. 745–782.
[18] V. Rives, Characterisation of layered double hydroxides and their decomposition products, Mater. Chem. Phys. 75 (2002) 19–25.
[19] V. Rives, D. Carriazo, C. Martín, Heterogeneous catalysis by polyoxometalate-Intercalated layered double hydroxides, in: A. Gil, A.S. Korili, R. Trujillano, A.M. Vicente (Eds.), Pillared Clays and Related Catalysts, Springer New York, New York, NY, 2010, pp. 319–397.
[20] C.E. Daza, C.R. Cabrera, S. Moreno, R. Molina, Syngas production from CO2 reforming of methane using Ce-doped Ni-catalysts obtained from hydrotalcites by reconstruction method, Appl. Catal. A Gen. 378 (2010) 125–133.
[21] D.P. Debecker, E.M. Gaigneaux, G. Busca, Exploring, tuning, and exploiting the basicity of hydrotalcites for applications in heterogeneous catalysis, Chem. Eur. J. 15 (2009) 3920–3935.
[22] United Nations Conference on Climate Change (COP21).
[23] A.R. Gonzalez, Y.J.O. Asencios, E.M. Assaf, J.M. Assaf, Dry reforming of methane on Ni-Mg-Al nano-spheroid oxide catalysts prepared by the sol-gel method from hydrotalcite-like precursors, Appl. Surf. Sci. 280 (2013) 876–887.
[24] O.W. Perez-Lopez, A. Senger, N.R. Marcilio, M.A. Lansarin, Effect of composition and thermal pretreatment on properties of Ni–Mg–Al catalysts for CO2 reforming of methane, Appl. Catal. A Gen. 303 (2006) 234–244.
[25] X. Lin, R. Li, M. Lu, C. Chen, D. Li, Y. Zhan, L. Jiang, Carbon dioxide reforming of methane over Ni catalysts prepared from Ni–Mg–Al layered double hydroxides: influence of Ni loadings, Fuel 162 (2015) 271–280.
[26] Y. Zhu, S. Zhang, B. Chen, Z. Zhang, C. Shi, Effect of Mg/Al ratio of NiMgAl mixed oxide catalyst derived from hydrotalcite for carbon dioxide reforming of methane, Catal. Today 264 (2016) 163–170.
[27] H. Liu, D. Wierzbicki, R. Debek, M. Motak, T. Grzybek, P. Da Costa, M.E. Gálvez, La-promoted Ni-hydrotalcite-derived catalysts for dry reforming of methane at low temperatures, Fuel 182 (2016) 8–16.
[28] C.E. Daza, J. Gallego, F. Mondragón, S. Moreno, R. Molina, High stability of Ce-promoted Ni/Mg–Al catalysts derived from hydrotalcites in dry reforming of methane, Fuel 89 (2010) 592–603.
[29] R. Dębek, M. Motak, D. Duraczyska, F. Launay, M.E. Galvez, T. Grzybek, P. Da Costa, Methane dry reforming over hydrotalcite-derived Ni-Mg-Al mixed oxides: the influence of Ni content on catalytic activity, selectivity and stability, Catal. Sci. Technol. 6 (2016) 6705–6715.
[30] R. Dębek, M. Radlik, M. Motak, M.E. Galvez, W. Turek, P. Da Costa, T. Grzybek, Ni-containing Ce-promoted hydrotalcite derived materials as catalysts for methane reforming with carbon dioxide at low temperature—on the effect of basicity, Catal. Today 257 (2015) 59–65.
[31] R. Dębek, K. Zubek, M. Motak, P. Da Costa, T. Grzybek, Effect of nickel incorporation into hydrotalcite-based catalyst systems for dry reforming of methane, Res. Chem. Intermed. 41 (2015) 9485–9495.
[32] R. Dębek, M.E. Galvez, F. Launay, M. Motak, T. Grzybek, P. Da Costa, Low temperature dry methane reforming over Ce, Zr and CeZr promoted Ni-Mg-Al hydrotalcite-derived catalysts, Int. J. Hydrogen Energy 41 (2016) 11616–11623.
[33] D. Wierzbicki, R. Dębek, J. Szczurowski, S. Basąg, M. Włodarczyk, M. Motak, R. Baran, Copper, cobalt and manganese: modified hydrotalcite materials as catalysts for the selective catalytic reduction of NO with ammonia. The influence of manganese concentration, C.R. Chim. 18 (2015) 1074–1083.
[34] S.Y. Foo, C.K. Cheng, T.-H. Nguyen, A.A. Adesina, Evaluation of lanthanide-group promoters on Co–Ni/Al2O3 catalysts for CH4 dry reforming, J. Mol. Catal. A Chem. 344 (2011) 28–36.
[35] R. Dębek, M. Motak, T. Grzybek, E.M. Galvez, P. Da Costa, A short review on the catalytic activity of hydrotalcite-derived materials for dry reforming of methane, Catalysts 7 (2017).
[36] L. Tian, X.H. Zhao, B.S. Liu, W.D. Zhang, Preparation of an industrial Ni-based catalyst and investigation on CH4/CO2 reforming to syngas, Energy Fuels 23 (2009) 607–612.
[37] D. Tichit, N. Das, B. Coq, R. Durand, Preparation of Zr-containing layered double hydroxides and characterization of the acido-Basic properties of their mixed oxides, Chem. Mater. 14 (2002) 1530–1538.
[38] S. Velu, V. Ramaswamy, S. Sivasanker, New hydrotalcite-like anionic clays containing $Zr4^+$ in the layers, Chem. Commun. (1997) 2107–2108.
[39] L. Chmielarz, A. Węgrzyn, M. Wojciechowska, S. Witkowski, M. Michalik, Selective catalytic oxidation (SCO) of ammonia to nitrogen over hydrotalcite originated Mg–Cu–Fe mixed metal oxides, Catal. Lett. 141 (2011) 1345–1354.
[40] L. Chmielarz, P. Kuśtrowski, A. Rafalska-Łasocha, D. Majda, R. Dziembaj, Catalytic activity of Co-Mg-Al, Cu-Mg-Al and Cu-Co-Mg-Al mixed oxides derived from hydrotalcites in SCR of NO with ammonia, Appl. Catal. B Environ. 35 (2002) 195–210.
[41] H. -p. Wu, W. -j. Li, L. Guo, Y. -f. Pan, X. -f. Xu, Effect of promoter species and precursors on catalytic activity of alkali metal promoted NiAl mixed oxides for N2O decomposition, J. Fuel Chem. Technol. 39 (2011) 550–555.
[42] H.-p. Wu, Z.-y. Qian, X.-l. Xu, X.-f. Xu, N2O decomposition over K-promoted NiAl mixed oxides derived from hydrotalcite-like compounds, J. Fuel Chem. Technol. 39 (2011) 115–121.
[43] B. Mile, D. Stirling, M.A. Zammitt, A. Lovell, M. Webb, The location of nickel oxide and nickel in silica-supported catalysts: two forms of NiO and the assignment of temperature-programmed reduction profiles, J. Catal. 114 (1988) 217–229.
[44] W. Gac, Acid–base properties of Ni–MgO–Al2O3 materials, Appl. Surf. Sci. 257 (2011) 2875–2880.
[45] J.I. Di Cosimo, V.K. Díez, M. Xu, E. Iglesia, C.R. Apesteguía, Structure and surface and catalytic properties of Mg-Al basic oxides, J. Catal. 178 (1998) 499–510.
[46] J.-H. Kim, D.J. Suh, T.-J. Park, K.-L. Kim, Effect of metal particle size on coking during CO2 reforming of CH4 over Ni–alumina aerogel catalysts, Appl. Catal. A Gen. 197 (2000) 191–200.